Journal of Cleaner Production 273 (2020) 122989

Contents lists available at ScienceDirect

Journal of Cleaner Production

journal homepage: www.elsevier.com/locate/jclepro

Critical insights into thermohaline stratification for geothermal energy recovery from flooded mines with mine water

Ting Bao [a, b, c], Han Cao [d], Yinghong Qin [a, e, *], Guosheng Jiang [f], Zhen (Leo) Liu [c, **]

[a] College of Civil Engineering and Architecture, Guangxi University, 100 University Road, Nanning, Guangxi, 540003, China
[b] Key Laboratory of Metallogenic Prediction of Nonferrous Metals and Geological Environment Monitoring (Central South University), Ministry of Education, 932 Lushan S Road, Changsha, Hunan, 410083, China
[c] Department of Civil and Environmental Engineering, Michigan Technological University, 1400 Townsend Drive, Houghton, MI, 49931, USA
[d] School of Geoscience and Info-Physics, Central South University, 932 Lushan S Road, Changsha, Hunan, 410083, China
[e] The Key Laboratory of Disaster Prevention and Structural Safety of Ministry of Education, Nanning, Guangxi, 530004, Chinaxi, 540003, China
[f] Engineering Faculty, China University of Geosciences (Wuhan), Wuhan, Hubei, 430074, China

A R T I C L E I N F O

Article history:
Received 17 June 2019
Received in revised form
15 June 2020
Accepted 20 June 2020
Available online 18 July 2020

Handling Editor: Yutao Wang

Keywords:
Mine water
Geothermal energy
Double-diffusive convection
Thermohaline stratification
Merging layers
Initial thermohaline distribution prediction

A B S T R A C T

Geothermal applications with waste water in abandoned mines are a sustainable way of recycling wastes in abandoned facilities for utilizing clean energy. Thermohaline stratification in mine water is significant to this energy application, because it dominates the heat and mass transport in the mine-water-geologic-formation system and consequently determines the efficiency and sustainability of geothermal energy systems. This study addresses six unresolved issues for understanding the formation and evolution of thermohaline stratification via multiphysics simulations, including effects of key transport parameters on thermohaline stratification; mechanisms underlying layer-merging; effects of the buoyancy ratio on thermohaline stratification, and predictions of the initial distributions of temperature and salinity for thermohaline stratification. Our results showed that the effective kinematic viscosity is the most dominant transport parameter to determine the layer-merging speed and layer number of thermohaline stratification, where seven more thermohaline stratification layers could be observed if two orders of magnitude of this parameter are increased. For layer-merging, relatively “weak” interfaces, which have a small buoyancy ratio across the neighboring layers, disappear and are eroded first. Our results also revealed that the buoyancy ratio determines the layer number, where increasing the buoyancy ratio from 2.16 to 4 can induce twenty more layers. The initially linear temperature and salinity distributions in mine water are needed for predicting the present and future thermohaline stratification, especially the energy recovery. To meet this need, an approach was proposed to accurately predict such initial distributions via back-calculating field measurements. This study provides insights into understanding the key energy transport mechanisms in mine water and recommendations for facilitating future implementations of geothermal energy recovery with mine water dominated by thermohaline stratification.

1. Introduction

Geothermal energy is a cleaner and renewable energy resource used for heating and cooling purposes with little environmental impacts (Esen and Yuksel, 2013; Radosław and Uliasz-Misiak, 2019). Recently, geothermal energy recovery from flooded mines has been receiving increasing research attention. Due to lodes in deep location, water in abandoned mines is heated by the Earth's geothermal energy, so abandoned mines can serve as large-scale reservoirs of warm water for providing low enthalpy heating energy with low-level carbon emissions for heating buildings (Watzlaf and Ackman, 2006), with some cases even for electricity generation (about 153–197 GWh/year) (Menéndez et al., 2019). Furthermore, mine water is usually treated as waste materials, it is thus sustainable, economical, and recyclable with waste materials and abandoned facilities for geothermal applications (Bakhtavar

* Corresponding author. College of Civil Engineering and Architecture, Guangxi University, 100 University Road, Nanning, Guangxi, 540003, China.
** Corresponding author. Department of Civil and Environmental Engineering, Michigan Technological University, 1400 Townsend Drive, Houghton, MI, 49931, USA.
E-mail addresses: yqin1@mtu.edu (Y. Qin), zhenl@mtu.edu (Z. Liu).
URL: http://www.liurg.org

https://doi.org/10.1016/j.jclepro.2020.122989
0959-6526/

Nomenclature

h	water height [m]
H	layer thickness [m]
$\mathbf{g}$	gravitational acceleration vector [m/s^2]
t	time [s]
p	total pressure [Pa]
p_d	hydrodynamic pressure [Pa]
T_0	reference temperature [K]
T	temperature [K]
T_t	top temperature [K]
T_b	bottom temperature [K]
r	aspect ratio [-]
w	shaft width [m]
$\mathbf{U}$	velocity [m/s]
S	salinity [%, w/w]
S_t	top salinity [%, w/w]
S_b	bottom salinity [%, w/w]
S_0	reference salinity [%, w/w]
z	elevation [m]

Dimensionless numbers

N	buoyancy ratio
λ	diffusivity ratio
Pr	Prandtl number
Ra	Rayleigh number
Ra_c	critical Rayleigh number
Ra_T	thermal Rayleigh number
Ra_S	solutal Rayleigh number
Sc	Schmidt number

Greek symbols

ρ_0	reference density [kg/m^3]
ρ	density [kg/m^3]
ν_{eff}	effective kinematic viscosity [m^2/s]
β_T	thermal expansion coefficient [K^{-1}]
β_S	solutal expansion coefficient [%$^{-1}$]
α_{eff}^T	effective thermal diffusivity [m^2/s]
α_T	thermal eddy diffusivity [m^2/s]
α_{eff}^S	effective solutal diffusivity [m^2/s]

et al., 2019).

Since the pioneering work for geothermal energy recovery from the Springhill coal mine in Canada (Jessop, 1995), mine water-based geothermal applications have been pioneered in some real projects around the world, such as Germany (Rottluff, 1998), Scotland (Burke, 2002), Spain (Rodríguez and Díaz, 2009), the U.K. (Burnside et al., 2016a), Netherlands (Behrooz et al., 2008), and the U.S. (Bao and Liu, 2019a; Bao et al., 2018a). Hall et al. (2011) reviewed existing assessment studies at specific sites and concluded that geothermal energy reserves in underground mines ranged from a few hundreds of kilowatts to hundreds of megawatts. Field measurements showed that 47.5 MW of thermal power (Bailey et al., 2016) and 260,000 MWh of annual thermal energy (Jardón et al., 2013) could be possible with mine water, and a real mine water-geothermal plant can produce 10 MW of thermal power (Menéndez et al., 2020). In real applications, the temperature of mine water is key to determining the efficiency of geothermal energy systems. Field testing results (Athresh et al., 2016; Farr et al., 2016) indicated that the water temperature available for geothermal applications ranged from 10.3 to 18.6 °C. Measurements at other sites also revealed relatively high average water temperatures of 12.8–24 °C contrast with the air temperature (Bao et al., 2019; Burnside et al., 2016b; Loredo et al., 2017). These studies showed the remarkable potential of geothermal energy recovery from flooded mines.

Though real projects and field measurements have been conducted extensively, attention is needed to understand the natural mine-water-geologic-formation system, especially the heat and mass transport in large bodies of mine water. The transport mechanisms and water temperature variations, particularly the subsequent water temperature distribution during heat extraction, determine the overall efficiency and sustainability of the whole geothermal energy system. As a common type of deep subterranean water bodies, mine water usually has a layered structure frequently observed in most flooded mines (Bao et al., 2018b; Johnson and Younger, 2002; Ladwig et al., 1984; Reichart et al., 2011; Wolkersdorfer, 2008). In this layered structure, both the temperature and salinity in mine water are stratified into different layers. Each layer has almost identical temperature and salinity, which is thus termed thermohaline stratification (see Fig. 1). Thermohaline stratification is a key to the better design and optimization of geothermal energy systems, because it dominates the heat and mass transport in mine water to determine the present and future water temperatures available to heat pumps, consequently, determining the overall efficiency and sustainability of the systems. Due to thermohaline stratification, the water at deeper locations is continuously heated by the Earth, which can provide a few gigawatt hours of annual energy (Wieber et al., 2019). In return, geothermal energy system parameters, such as water pumping locations (Zhang et al., 2019) and pumping rates (Luo et al., 2018), will alter the water temperature and its variations. The selection of these parameters will influence the energy and mass transport dominated by thermohaline stratification and consequently the overall performance of the system. Therefore, a sound understanding is thus needed for engineering designs of geothermal energy systems with mine water, especially for quantifying the influences of pumping rates and locations, long-term sustainability and environment considerations, and the interaction between the natural system and the geothermal energy system.

Double-Diffusive Convection (DDC) is believed to be major heat and mass transport mechanisms determining the formation of thermohaline stratification in mine water (Brandt and Fernando, 1995). For DDC in most mine water bodies, cold and fresh water overlies warm and salty water due to geothermal (temperature) and geochemical (salinity) gradients. In this condition, the bottom water with a high salinity can suppress thermal convection in the vertical direction. This is because the bottom water moves up while the top water moves down because the bottom water is less dense than the top water. Because of the co-existence of the salinity gradient, a high salinity makes that bottom water more dense than the fresh water at the top. Meanwhile, the geothermal gradient turns to make the bottom water less dense. Therefore, temperature and salinity in mine water contribute oppositely, and a sound understanding of DDC is thus significant to geothermal energy recovery with large subterranean water bodies.

A few studies have investigated the formation and evolution of thermohaline stratification via DDC simulations. Reichart et al. (2011) numerically modeled DDC flow patterns of mine water. However, thermohaline stratification was not successfully observed, and the sale of mine water was very small (i.e., 1 m) in their model. Therefore, such a scale is not realistic for real mines, i.e., 1 km or greater. Kories et al. (2004) successfully reproduced thermohaline stratification via DDC in large bodies of mine water

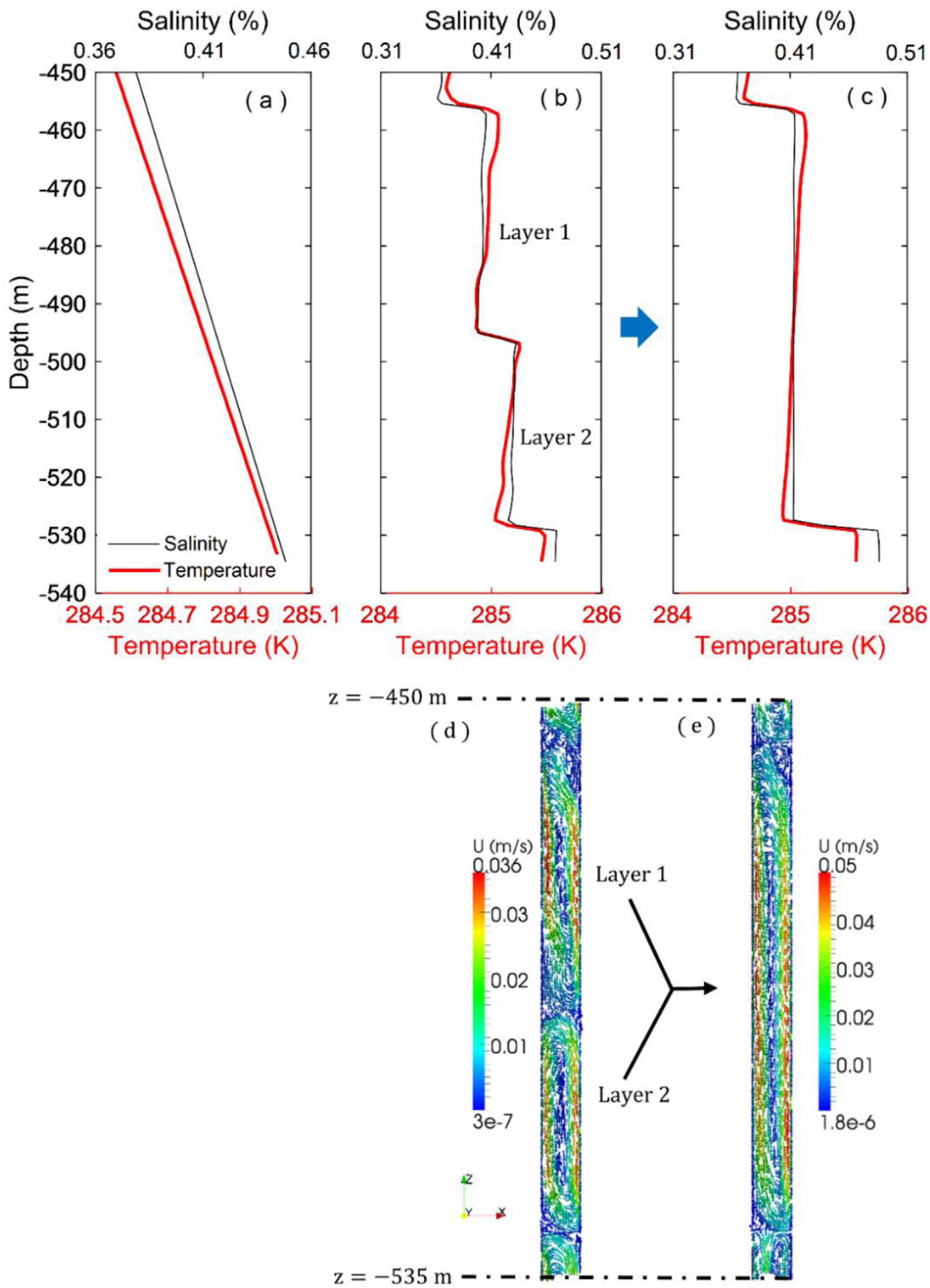

Fig. 1. Formation and evolution of thermohaline stratification in mine water. The presented results were obtained from the simulation of Hancock Shaft 2 in a depth range between −450 m and −535 m (water surface = 0). The distributions of temperature and salinity along the shaft axis were obtained at (a) 0 (initial condition), (b) 6 h, and (c) 12.5 h. The corresponding flow patterns for (b) and (c) are presented in (d) and (e). In this example, the buoyancy ratio $N = 2$ and the diffusivity ratio (heat/salt) $\lambda = 1/500$.

(around 0.75 km). Their stratification was obtained based on a condition that the salinity was stratified initially, which however is not true in reality. Bao and Liu (2019b) succeeded in reproducing thermohaline stratification in large bodies of mine water (around 1.2 km). Fig. 1 presents an example of the formation and evolution of thermohaline stratification. The distributions of temperature and salinity are initially linear (Fig. 1a), and then, two layers spontaneously form (see Fig. 1b). Water circulates in each layer individually (Fig. 1d), and there are significant temperature and salinity differences between adjacent layers (Fig. 1b). As time elapses, Layer 1 and Layer 2 merge to form one layer with a greater thickness (Fig. 1c and e).

Despite the above progress, an in-depth understanding of the heat and mass transport dominated by thermohaline stratification is still limited. In particular, six issues remain unresolved: (1–3) the effect of the key transport parameters, i.e., effective thermal diffusivity, effective kinematic viscosity, and diffusivity ratio, on thermohaline stratification; (4) mechanisms underlying the layer-merging event; (5) the effect of the buoyancy ratio on thermohaline stratification; and (6) the accurate prediction of the initial distributions of temperature and salinity, which are needed for predicting the present and future thermohaline stratification, especially the energy recovery from real flooded mines. These six issues slow down the widespread adoption of this energy application with mine water, because thermohaline stratification determines temperature variations in mine water to either negatively or positively affect the overall sustainability and efficiency of real geothermal applications. However, the characteristics of thermohaline stratification are little understood. Furthermore, from a practical perspective, addressing these six issues can provide useful recommendations for geothermal system designs. Such recommendations to facilitate this energy application, however, are lacking in existing numerical studies.

This study thus addresses the above six issues via multiphysics simulations. The objective is to provide in-depth insights for understanding the dominant energy and mass transport mechanisms in mine water. Although the theory of multiphysics simulations in this study is the same as that in Bao and Liu (2019b), we conduct new sensitivity analyses here to understand the characteristics of thermohaline stratification. Based on that, we will provide useful recommendations that have not been reported before for engineering designs of geothermal energy systems to facilitate geothermal applications with mine water. The organization of this study is detailed as follows. A scientific framework for non-isosolutal and non-isothermal hydrodynamics is presented in Section 2.1 and validated against the documented results in Section 2.2. Multiphysics simulations are conducted in Section 3.1 for a real flooded mine shaft. Based on the simulations, the above six issues are investigated separately in Section 3, and discussions are detailed in Section 4.

2. Theory and method

2.1. Theoretical framework

This section presents a theoretical framework for modeling DDC in mine water. The continuity equation is formulated as

$$\nabla \cdot \mathbf{U} = 0 \tag{1}$$

where $\mathbf{U}$ is the water velocity. The momentum equation is formulated by

$$\frac{\partial \mathbf{U}}{\partial t} + \mathbf{U} \cdot \nabla \mathbf{U} = -\frac{\nabla p_d}{\rho_0} + \nabla \cdot \left(\nu_{eff} \nabla \mathbf{U}\right) + \frac{\rho}{\rho_0}\mathbf{g} \tag{2}$$

where ν_{eff} is the effective kinematic viscosity; ρ is the water density; ρ_0 is the reference water density; $\mathbf{g}$ is the gravitational acceleration vector; $p_d = p - \rho g z$, which is the hydrodynamic pressure; p is the total pressure; z is the depth; and the absolute value of $\rho g z$ is the hydrostatic pressure. The Oberbeck-Boussinesq approximation (Sezai and Mohamad, 2000) was used to consider the buoyancy force induced by temperature and salinity differences. With this approximation, the density ρ varies linearly with the water temperature T and solute concentration (i.e., salinity) S as

$$\rho = \rho_0[1 - \beta_T(T - T_0) + \beta_S(S - S_0)] \tag{3}$$

where β_T is the coefficient of thermal expansion; β_S is the coefficient of solutal expansion; and T_0 and S_0 are the reference temperature and salinity, respectively.

The energy equation is formulated as

$$\frac{\partial T}{\partial t} + \mathbf{U} \cdot \nabla T = \nabla \cdot \left(\alpha_{eff}^T \nabla T\right) \tag{4}$$

where α_{eff}^T is the effective thermal diffusivity. The salinity equation is governed by

$$\frac{\partial S}{\partial t} + \mathbf{U} \cdot \nabla S = \nabla \cdot \left(\alpha_{eff}^S \nabla S\right) \tag{5}$$

where α_{eff}^S is the effective solutal diffusivity.

The water movement is caused by temperature and salinity differences, which affect the buoyancy force in the dynamic DDC system. The buoyancy ratio N is used to assess the relative influence of salinity and temperature on the buoyancy force as

$$N = \frac{\beta_S \Delta S}{\beta_T \Delta T} \tag{6}$$

Turbulent flow is common in mine water (Wolkersdorfer, 2008). To consider this, we assumed constant effective kinematic viscosity and effective diffusivity values. This assumption is similar to that employed in the numerical modeling of water circulations in oceans with constant transport parameters, e.g., Radko et al. (2014a). For both thermal and solutal diffusion, the effective diffusivity is the sum of the laminar diffusivity and the eddy diffusivity. The thermal eddy diffusivity α_T can be estimated with Eq. (7) (Vallis, 2017)

$$\overline{\mathbf{U}'T'} = -\alpha_T \nabla T \tag{7}$$

where $\overline{\mathbf{U}'T'}$ is the eddy flux. According to Wolkersdorfer (2008), the maximum water velocity measured from tracer tests was in an order of 10^{-2} m/s. α_T thus can be assessed with this velocity magnitude. Similarly, we can estimate the solutal eddy diffusivity by replacing T and T' in Eq. (7) with S and S'. The effective kinematic viscosity is also the sum of the laminar kinematic viscosity and the eddy kinematic viscosity. The eddy kinematic viscosity can be computed based on the turbulent Prandtl number and the eddy thermal diffusivity. Those transport parameters used in this study are detailed in Table 1 later in Section 3.1. The governing equations listed above were discretized and solved using OpenFOAM (OpenFOAM, 2009) with the PISO algorithm (Oliveira and Issa, 2001).

2.2. DDC framework validation

The above DDC framework was validated here against the documented results. In detail, the published numerical study (Han and Kuehn, 1991b) with the laminar flow reproduced experimentally observed steady-state DDC in water in an enclosure (Han and Kuehn, 1991a). The model setup is shown in Fig. 2a. The vertical-horizontal ratio is 4.0. The left side was fixed with T_t (low temperature) and S_b(low salinity); while the right side was fixed with T_b (high temperature) and S_b (high salinity). The top and bottom sides were set up with no heat and salt fluxes. The initial conditions

Table 1
Parameters used in the DDC simulation for water in Hancock Shaft 2.

Material	Parameter	Value
Mine water	Reference temperature (K)	333.15
	Reference salinity (%)	15
	Reference density (kg/m^3)	1088.6
	Thermal expansion coefficient (K^{-1})	5.24×10^{-4}
	Solutal expansion coefficient (%$^{-1}$)	6.82×10^{-3}
	Effective kinematic viscosity (m^2/s)	3.95×10^{-3}
	Effective salty diffusivity (m^2/s)	1×10^{-6}
	Effective thermal diffusivity (m^2/s)	4.93×10^{-4}
	Specific heat (J/(kg K))	4181

Note: Solutal and thermal properties of mine water are determined according to Hull et al. (1988); reference temperature and salinity are used in Eq. (3).

of temperature and salinity in water were uniform T_t and S_b, respectively. The above initial and boundary values for temperature and salinity were calculated based on the buoyancy ratio N and the thermal Rayleigh number Ra_T strictly following Han and Kuehn (1991b). The adopted parameters were $N = 7.5$; $Ra_T = 3.2 \times 10^6$; the Prandtl number $Pr = 8$; and the Schmidt number $Sc = 2000$. The simulation was conducted until temperature and salinity reached the quasi-steady state. Fig. 2b and c shows the comparisons of the distributions of dimensionless temperature and salinity along the vertical center axis of water. The temperature and salinity distributions obtained in this study are in agreement with the published numerical results, which indicates the good capacity of the framework proposed in this study for simulating the natural DDC process.

2.3. Model development and thermohaline stratification

This section details thermohaline stratification modeling of a real flooded mine. Hancock Shaft 2 in the Upper Peninsula of Michigan was flooded with water soon after its closure. Thermohaline stratification was observed in water in this shaft from field measurements (Bao et al., 2018b), in which temperature and salinity (indirectly measured by electrical conductivity) were stratified into at least two distinct layers along the vertical axis of Shaft 2. This shaft was chosen in this study to understand the key mass and heat transport mechanisms dominated by thermohaline stratification.

Fig. 3 shows the 2D model configuration (Fig. 3b) developed based on the realistic layout of Hancock Shaft 2 (Fig. 3a). The model consists of one vertical shaft with a width of 5.8 m and a depth of 1159.2 m. The shaft connects eight horizontal drifts with a length of 50 m. The model geometry was meshed with a resolution of 0.36 m and 0.4 m in the horizontal and vertical directions, respectively, for water in the shaft and drifts. A higher resolution of 0.01 m was adopted on the lateral boundaries of the model to avoid numerical stability issues in the consideration of the boundary conditions. The boundary conditions were implemented with lateral heat fluxes from the surrounding rocks and also from the water flows through

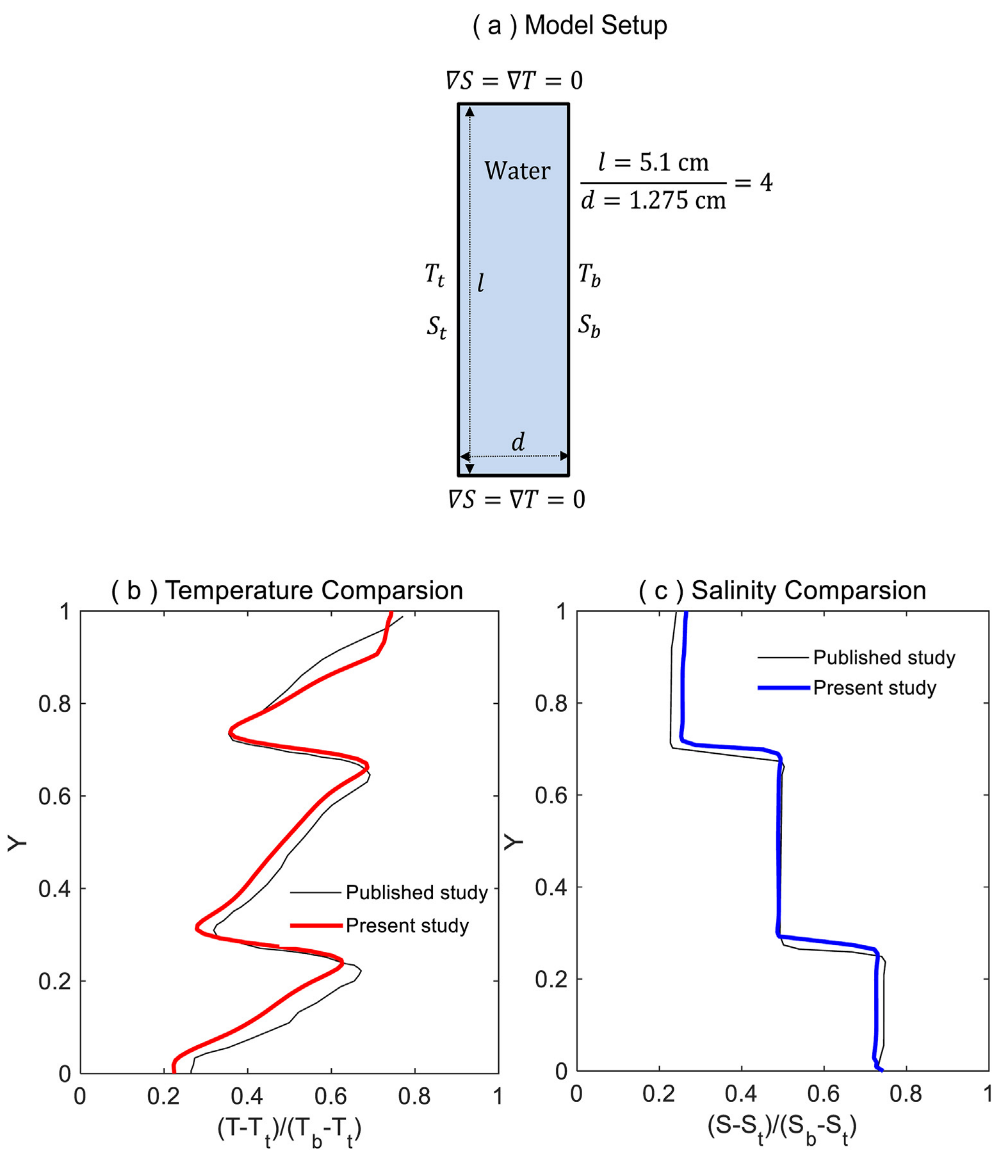

Fig. 2. Comparisons between the present results and the published numerical results (Han and Kuehn, 1991b): (a) model setup, (b) dimensionless temperature, and (c) dimensionless salinity.

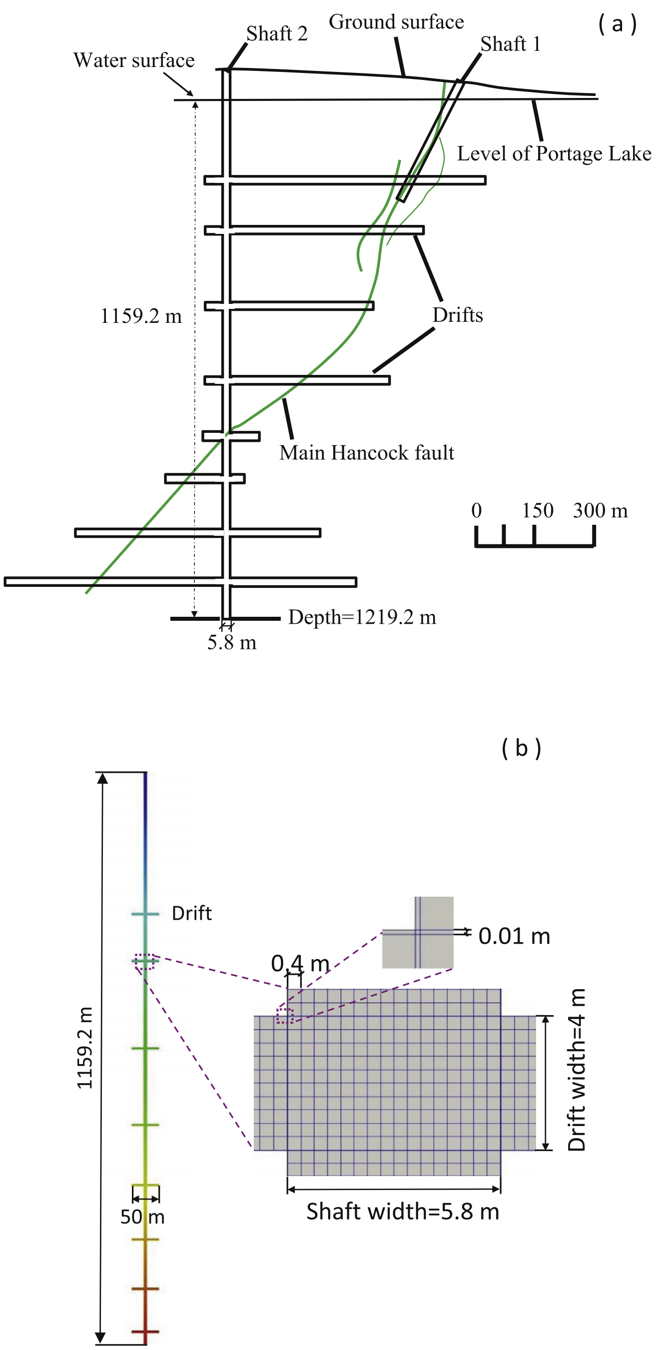

Fig. 3. Hancock Shaft 2: (a) underground structure layout [modified after (Butler and Burbank, 1929)] and (b) model configuration and its grid.

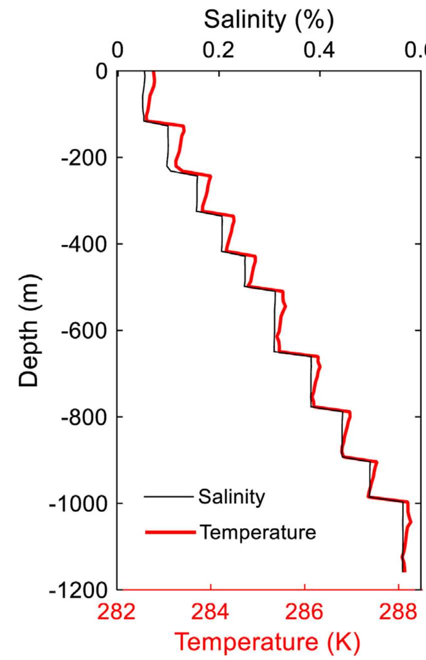

Fig. 4. Thermohaline stratification in mine water along the center axis of Shaft 2 at t = 13 h when N = 1.26.

cracks and fissures in rocks to enter the shaft. In the implementation, the heat fluxes from rocks on both sides of mine water were identical because of the same geothermal gradient. For the water flows through cracks and fissures in rocks, there was a difference between their lateral heat fluxes on two sides of mine water due to the overall groundwater movement. More details for implementing the lateral heat fluxes can be found in Bao and Liu (2019b).

For the initial condition, the temperature was linearly distributed, i.e., from 282.15 K at the top to 288.35 K at the bottom according to field observations (Bao et al., 2018b). The salinity distribution was also linear. The top salinity S_t was assumed to be 0.01%, while the bottom salinity S_b was calculated using Eq. (6) with a prescribed buoyancy ratio N. For example, when N is assumed to be 1.26 (estimated according to the local hydrologists as freshwater from Lake Superior is plentiful in the study area), S_b is 0.61%. A sodium chloride solution was adopted to represent salinity in mine water because sodium chloride is the primary chemical component experimentally detected in mine water (Bao et al., 2018b). The thermal and solutal properties of mine water used in the simulation are detailed in Table 1. It is noted that the effective thermal and solutal water properties were estimated by considering the turbulence effect (see Eq. (7) for α_T determination) because such an effect is required for modeling thermohaline stratification (Bao and Liu, 2019b).

Thermohaline stratification can be observed in Fig. 4 when $N = 1.26$. Each layer has almost the same temperature and salinity. There are significant temperature and salinity differences between two adjacent layers. The layer numbers and depths are the same for both the temperature and salinity. The layers in Fig. 4 arise from the dynamic DDC process with the intrusion caused by the lateral heat flux (Bao and Liu, 2019b). To evaluate the dominant heat and solute transport mechanism (i.e., diffusion or convection) in the DDC process, the Rayleigh number Ra is compared with the critical Rayleigh number Ra_c. Because of the co-existence of temperature and salinity, Ra formulated by Eq. (8) is the sum of the thermal Ra_T and solutal Ra_S

$$Ra = Ra_T + Ra_S = \frac{g\beta_T(T_b - T_t)w^3}{\alpha_{eff}^T \nu_{eff}} + \frac{g\beta_S(S_b - S_t)w^3}{\alpha_{eff}^S \nu_{eff}} \tag{8}$$

where w is the shaft width. According to Love et al. (2007), the critical Rayleigh number Ra_c in DDC for the onset of convection in a vertical shaft can be estimated as

$$Ra_c = \frac{215.6}{r^4}\left(1 + 3.84r^2\right) \tag{9}$$

where r is the width-height ratio (w/h) and h is the mine water height. With the parameters detailed in Table 1, $Ra = 1.99\times 10^9$ is lower than $Ra_c = 3.44 \times 10^{11}$. Therefore, diffusion is predominant in the DDC process. This explains the observed stratification in Fig. 4. If convection dominates, temperature and salinity in a shaft will mix very quickly into one layer, e.g., buoyancy-driven flow in a vertical shaft (Bao et al., 2018b) and an inclined shaft (Bao and Liu, 2016). Therefore, layers could disappear very quickly or even not be observed in the DDC process if convection dominates.

3. Results

The results are presented in the following subsections to address the six unresolved issues mentioned in the introduction. Sections 3.1-3.3 and 3.5 investigate the effect of three transport parameters and the buoyancy ratio on thermohaline stratification. Section 3.4 discusses the layer-merging mechanism. The prediction of initial thermohaline stratification conditions is presented in Section 3.6. It is noted that a buoyancy ratio $N = 1.26$ was used everywhere except in Section 3.6, in which different N values were estimated according to local hydrologists to understand the influence of this factor. Since the numbers and depths of layers for temperature and salinity are identical (see Fig. 4), only temperature results are presented while salinity results will be presented only if necessary.

3.1. Effect of effective thermal diffusivity

Thermohaline stratification in Fig. 5 was obtained when Ra_T is 3.19×10^6 and the corresponding effective thermal diffusivity α^T_{eff} is 4.93×10^{-4} m^2/s. It was explained in Section 2.3 that diffusion needs to dominate in the dynamic DDC process so that we can produce thermohaline stratification. In heat diffusion, the effective thermal diffusivity α^T_{eff} is a key transport parameter and its influence on thermohaline stratification is thus investigated in this section. For this purpose, α^T_{eff} varies while all the other parameters remain unchanged.

The effective thermal diffusivity determines the layer formation speed. As shown in Fig. 5, at $t = 3$ h when $\alpha^T_{eff} = 4.93$e-5 m^2/s, no layers can be observed in Fig. 5a. However, when α^T_{eff} increases to 4.93e-4 m^2/s and 1.56e-3 m^2/s, at least six layers can be seen in Fig. 5c and more layers (about thirteen) are observed in Fig. 5d. At $t = 13$ h, layers can be seen in all the considered cases with different α^T_{eff} values, in which the difference is the layer number. Therefore, the higher the effective thermal diffusivity, the faster the layered water structure forms.

3.2. Effect of effective kinematic viscosity

The effective kinematic viscosity ν_{eff} is another key transport parameter in determining the speed of fluid movement. In this section, the influence of ν_{eff} on stratification processes with different ν_{eff} values is investigated.

The layer number increases as ν_{eff} increases. As shown in Fig. 6, the layer number increases from seven to fourteen when ν_{eff} increases from 3.95×10^{-4} m^2/s to 1.25×10^{-2} m^2/s. The reason is that a higher ν_{eff} value provides stronger resistance to the fluid movement. As a result, the water movement caused by convection with a higher ν_{eff} value is less significant than that with a lower value. Due to this reason, the mixing of temperature and salinity in the layer-merging process becomes slower if ν_{eff} increases, leading to a greater layer number.

3.3. Effect of diffusivity ratio

This section investigates the influence of the effective solutal diffusivity α^S_{eff} on thermohaline stratification because α^S_{eff} is an important transport parameter in determining the strength of salinity diffusion. Due to the co-existence of heat and salt diffusion, it is more helpful to indirectly investigate the influence of α^S_{eff} by

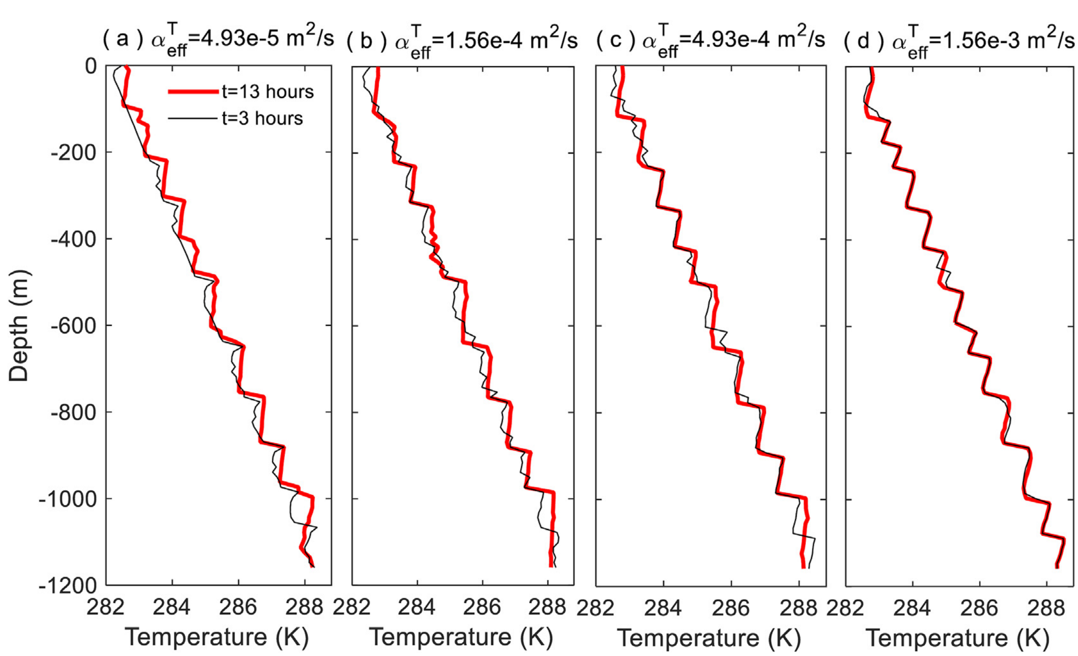

Fig. 5. Formation of temperature layers with different α^T_{eff} values at two different times. Corresponding Ra_T values are (a) 3.19×10^7, (b) 1.01×10^7, (c) 3.19×10^6, and (d) 1.01×10^6.

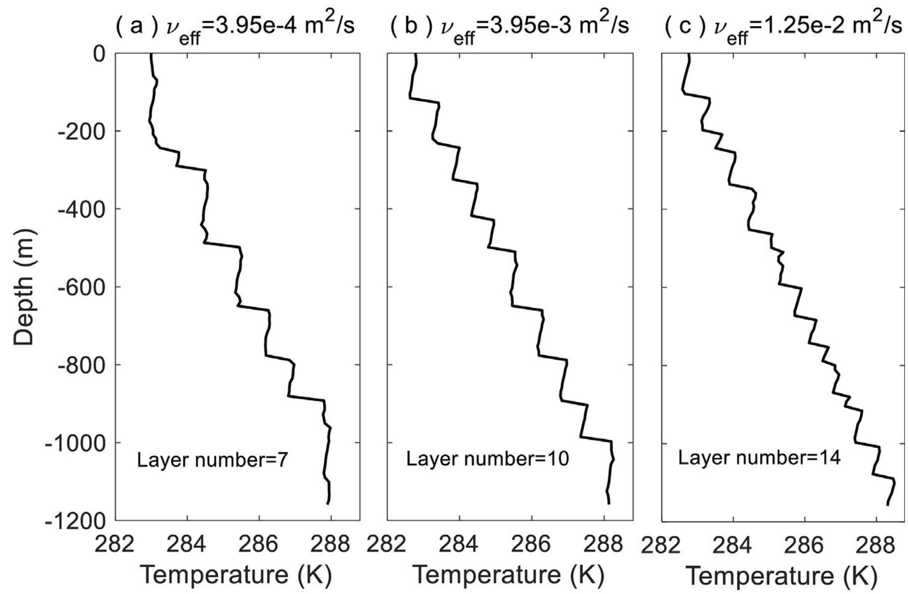

Fig. 6. Temperature layers with different values of ν_{eff} at $t = 13$ h.

understanding the influence of the diffusivity ratio (heat/solute) $\lambda = \alpha^T_{eff}/\alpha^S_{eff}$ on thermohaline stratification. According to the literature for modeling the dynamic DDC process in oceans (Carpenter et al., 2012), λ should be lower than 1.0 (i.e., heat diffuses faster than salt). Therefore, λ values smaller than 1.0 were considered in this section. To obtain different λ values, α^S_{eff} varies while α^T_{eff} remains unchanged.

The diffusivity density ratio controls the layer-merging speed to determine the layer number. Fig. 7 demonstrates the comparisons of temperature layers obtained with four different λ values, i.e., 1/6, 1/50, 1/250, and 1/1000. The layer number increases from eight to ten when λ decreases from 1/6 to 1/1000. The observations in Fig. 7 imply that the layer number is greater if the λ value is smaller.

3.4. Mechanisms underlying layer-merging

Layer-merging can be distinctly observed in the evolution of thermohaline stratification in mine water (see Fig. 1). However, mechanisms underlying layer-merging have rarely been investigated. This section aims to provide insights into such mechanisms in large bodies of mine water.

Considering that the scale of mine water is too large to visualize, we adopted -875~-1159.2 m depth range, which is representative in thermohaline stratification, to understand layer-merging. Fig. 8 illustrates thermohaline stratification and their corresponding flow patterns at different times in this depth range. There are three clear layers at $t = 300$ min (Fig. 10a). Water circulates in each layer and the water velocity is very small (around 7×10^{-9} m/s) at the interface between adjacent layers. When the layer-merging starts at $t = 360$ min (Fig. 10b), the water movement tends to break the interface of Layer 1 and Layer 2. The heat and solute within Layer 1 and Layer 2 mix gradually due to convection. As a result, this interface is eroded (Fig. 10b) and gradually disappears, leading to one layer with a greater thickness (Fig. 10c).

It also can be seen in Fig. 10b that the merging of Layers 1 and 2 occurs along the horizontal direction. This horizontal merging process matches the "B-mode" for merging layers according to the

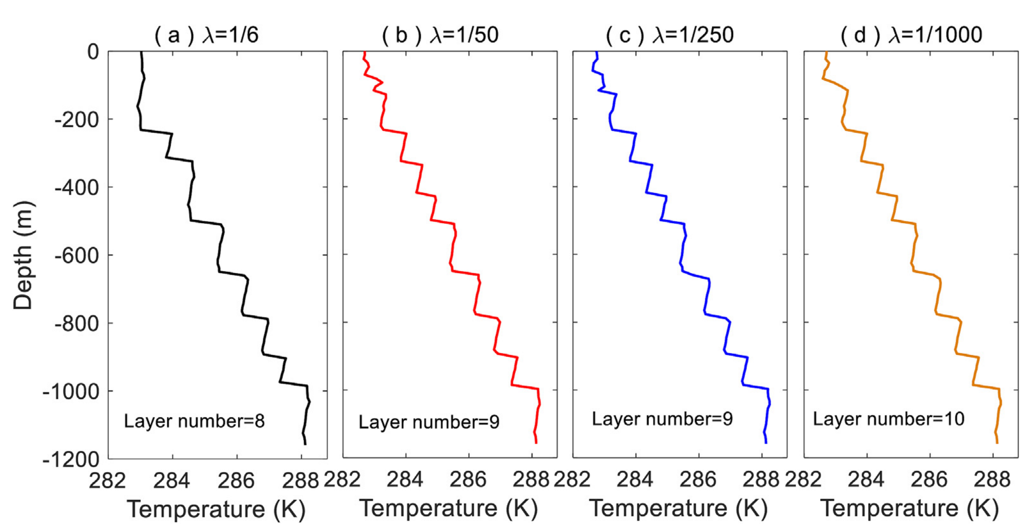

Fig. 7. Comparisons of temperature layers without considering the lateral salinity flux under different diffusivity ratios at $t = 16$ h.

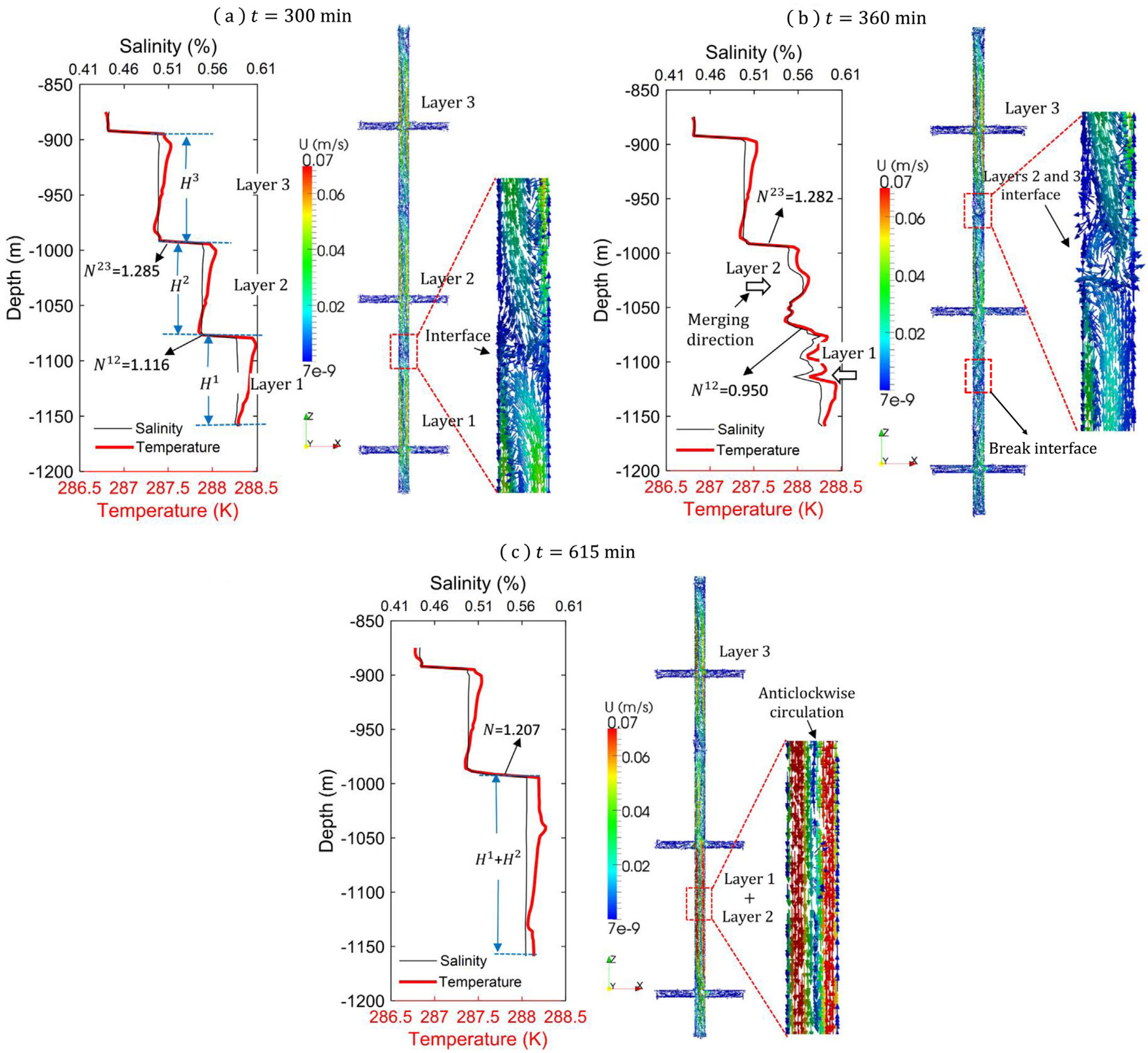

Fig. 8. Layer-merging process in the evolution of thermohaline stratification and their corresponding flow patterns at (a) 300 min, (b) 360 min, and (c) 615 min. The thermohaline stratification and their corresponding flow patterns were obtained in the depth range between −875 m and −1159.2 m.

classification of layer-merging modes (Radko et al., 2014b). The "B-mode" thus dominates layer-merging in the current simulation. It is noted that the merging process of Layers 1 and 2 does not hurt the interface of Layers 2 and 3 because the location of the interface and the thickness of Layer 3 almost remain unchanged, as shown in Fig. 10b and c.

Layer-merging in mine water in Fig. 8 possibly shares similar mechanisms with that in thermohaline staircases in oceans. According to a layer-merging theory in oceans (Radko, 2007), layer-merging via the erosion of "weak" interfaces occurs when the vertical buoyancy flux decreases with the buoyancy variation across those "weak" interfaces. This theory implies that the variation of the difference in the buoyancy force across an interface between adjacent layers determines if such an interface will be eroded or not. In the dynamic DDC process in mine water, the difference in the buoyancy force across an interface is determined by the buoyancy ratio that controls the convection process. The buoyancy ratio across any interface determines the buoyancy force in its two adjacent layers. If that buoyancy ratio decreases, the salinity difference between these two adjacent layers decreases. This reduces the suppression to the thermal convection caused by the salinity difference. Consequently, the difference in the buoyancy force between these two layers decreases. Thus, in Fig. 8, the variation of the buoyancy ratio N across the interface between Layers 1 and 2 primarily controls layer-merging.

To further quantitatively illustrate the variation of the buoyancy ratio during layer-merging processes, we calculated two buoyancy ratios N^{12} and N^{23} across two representative interfaces of Layers 1 and 2 and Layers 2 and 3 using Eq. (6). The calculation adopted the average values of temperature and salinity of the three layers with a

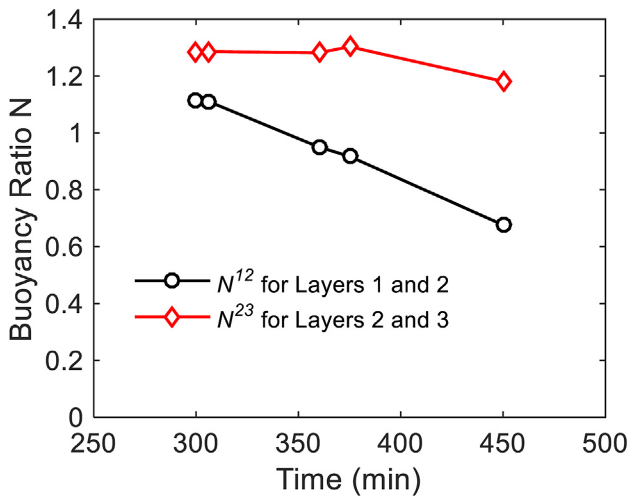

Fig. 9. Variations of buoyancy ratios with time across two representative interfaces during the layer-merging process.

thickness of H^1, H^2 and H^3 in Fig. 9a. For simplicity, it was assumed that those three thicknesses remain unchanged. As shown in Fig. 9a, the buoyancy ratios across the interfaces are $N^{12} = 1.116$ and $N^{23} = 1.285$. Because of $N^{23} > N^{12}$, the interface of Layers 1 and 2 is weaker, which will be eroded first. This explains why the layer-merging process does not hurt the interface of Layers 2 and 3 in Fig. 8. At $t = 360$ min, N^{12} decreases to 0.950 (by 14.9%). N^{12} further decreases during the layer-merging process (see Fig. 9). N^{23} also slightly decreases with time (by 4.8%). This is because both the temperature and salinity in Layer 2 increase when Layers 1 and 2 are merging, in which the increase in temperature is more significant than that in salinity. By contrast, the temperature and salinity in Layer 3 almost remain unchanged, leading to a decrease in N^{23} as well. However, the decrease in N^{12} is much greater than that in N^{23} because the interface of Layers 1 and 2 is weaker than that of Layers 2 and 3. Therefore, this "weaker" interface is eroded and disappears first. In summary, the smallest value of N corresponds to the "weakest" interface, which will be eroded first.

3.5. Effect of buoyancy ratio

The buoyancy ratio determines the overall heat and mass transport in the vertical direction and also controls the layer-merging as explained in Section 3.4. The effect of the buoyancy ratio on thermohaline stratification is thus investigated in this section. To consider its effect, ΔT (i.e., 6.2 K) and S_t (i.e., 0.01%) remain unchanged while S_b varies to obtain three different N values (i.e., 1.26, 2, and 4) assumed according to local hydrologists.

The buoyancy ratio determines the layer number in thermohaline stratification. As shown in Fig. 10, the layer number increases when the buoyancy ratio increases from 1.26 to 4. However, the smaller the buoyancy ratio, the less the layer number. This is because the layer-merging process with a high buoyancy ratio is much slower than that with a low one, leading to more but thinner layers. Therefore, the layer-merging process is very slow with a high buoyancy ratio.

3.6. Predicting initial conditions of thermohaline stratification

Field observations from flooded mines proved the widespread existence of temperature and salinity layers in mine water (Wolkersdorfer, 2008). For geothermal applications with mine water, predicting the development of the layered water structure is essential to tell us temperature variations and distributions in mine water, which is the key to the efficiency and sustainability of a geothermal energy system. However, the first step of such predictions in numerical simulations calls for the acquisition of field conditions, especially the initial distributions of temperature and salinity in mine water. Without correct initial conditions, the predicted layers will not evolve in a realistic way. To resolve this, we propose an approach by analyzing the field observed temperature and salinity and based on that, predicting the initial temperature

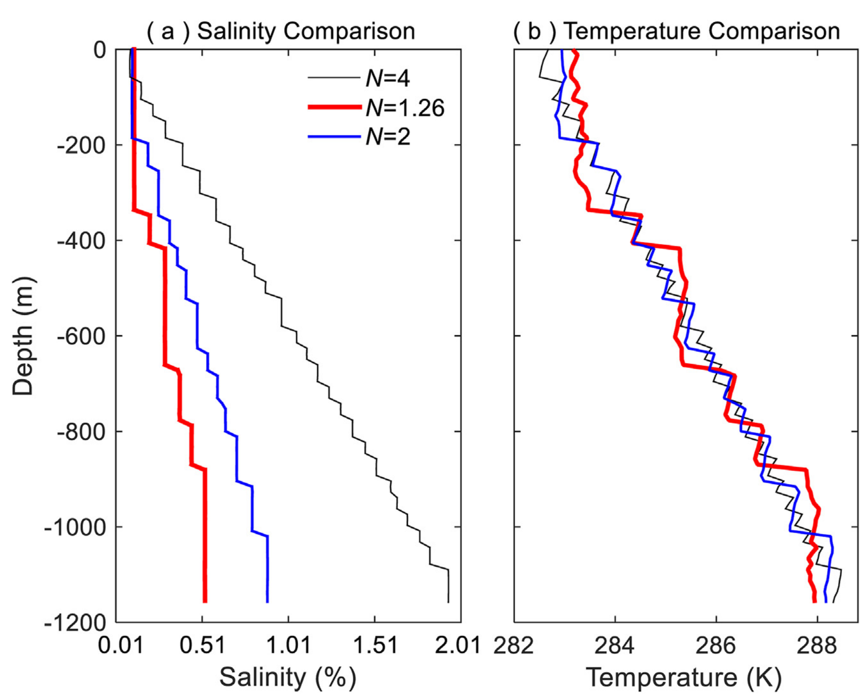

Fig. 10. Effect of buoyancy ratios on thermohaline stratification at $t = 2.5$ days (a) salinity comparison and (b) temperature comparison.

and salinity distributions. It was assumed that the initial temperature and salinity in mine water are linearly distributed due to geothermal and geochemical gradients according to Reichart et al. (2011).

In this approach, we predict the initial distributions by back-calculating the temperature and salinity picked from the observed layers in field measurements. Fig. 11 shows the way of data pick-up and calculations of temperature and salinity coordinates. For each layer and interface, the center coordinates are calculated first. All the centers of layers and interfaces are then utilized to predict the initial distributions based on the linear regression.

To evaluate the proposed approach, we tested three cases shown in Fig. 12 with different layer numbers. The cases correspond to $t = 25$ h (Case 1), 2.5 days (Case 2), and 4.5 days (Case 3), and their layer numbers are nine, six, and three, respectively. The above different layer numbers were adopted to consider field conditions with different layer numbers (Wolkersdorfer, 2008). The initial distributions of temperature and salinity, which were used to obtain the results in Fig. 12, will be treated as the true distributions and compared against the predicted distributions. The linear least-squares approach was used for the linear regression.

The predicted initial temperature distributions are in good agreement with the true initial distribution (see Fig. 13a). The predictions in Cases 1, 2, and 3 highly coincide with the true solution. The difference between the predicted and true temperature is in general about 0.2 K. The error analysis presented in Fig. 13b further proves that the error of the predictions is very small. The ratios between the predicted and true temperatures are almost equal to 1.0 for all the cases.

The initial salinity distributions can also be accurately predicted with the proposed approach. As can be seen in Fig. 14a, the predictions for the three cases almost overlap the true initial distribution, especially those of Case 1 and Case 2. The error analysis illustrated in Fig. 14b also indicates that the salinity predictions are accurate in Cases 1 and 2, in which the ratios of the predicted and true salinity values are very close to 1.0. Though there is a difference in the salinity prediction in Case 3, this difference is very small because the ratio difference is less than 0.025 (Fig. 14b). The results in Figs. 13 and 14 confirm the feasibility of predicting the initial linear distributions of temperature and salinity and also prove the high reliability and accuracy of the proposed approach.

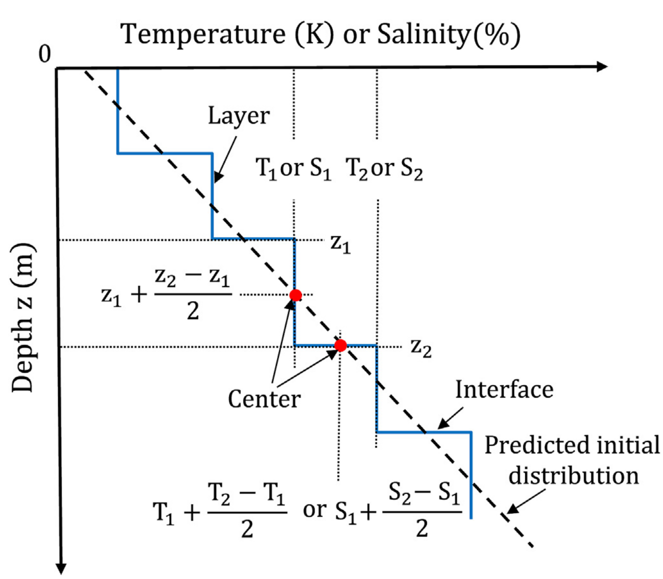

Fig. 11. Schematic of data pick-up and calculations of temperature and salinity coordinates.

4. Discussion

The insights in Section 3 have neither been reported nor considered in existing geothermal energy applications with mine water. However, such insights are essential to understanding the key energy and mass transport mechanisms dominated by thermohaline stratification from a scientific perspective. Furthermore, these insights are significant for guiding future geothermal system designs for better utilizing mine water-based geothermal energy from a practical perspective.

4.1. Insights to explain field observations

The results presented in Section 3.1-3.5 can explain field observations that are little understood. One critical but inexplicable field observation is that the layered water structure observed in many flooded mines, e.g., Vouters Shaft 2 (Reichart et al., 2011) and others (Wolkersdorfer, 2008), can remain relatively stable with an unchanged number of layers for a long time. This observation can be explained with the simulation results for the buoyancy ratio effect revealed in this study. As indicated in Fig. 10, a high buoyancy ratio will make the layer-merging process very slow. As a result, a higher ratio could lead to an unchanged number of layers over a long period. This observation can also be explained by the sensitivity analysis with the effective kinematic viscosity ν_{eff}, which also significantly influences the layer-merging speed, as revealed by the simulation in Section 3.2. In real mine water bodies, ν_{eff} could not be a constant (physically true), but rather be a variable that can increase to a very high value, depending on the natural water velocity and the water temperature difference caused by geothermal gradients. Consequently, water layers merge very slowly and the layer number can remain unchanged for a long time. Though it is difficult to prove using field tests, this could be examined with a simple numerical case shown in Fig. 15, in which ν_{eff} increases from a low value to a high one. Fig. 15a shows the comparison of layers obtained at different times with the same ν_{eff}. The number of layers decreases from nine to six from 1 day to 2.5 days. However, the layer number remains unchanged when ν_{eff} increases from 3.95×10^{-3} m^2/s to 1.25×10^{-2} m^2/s (Fig. 15b). Therefore, increasing ν_{eff} can significantly slow down the layer-merging process and enable the layer number to stay unchanged for a long time. In real mine water bodies, ν_{eff} is very likely to increase to a high value. This is because a higher value of ν_{eff} is needed to obtain a lower value of the Rayleigh number Ra (see Eq. (8)) to ensure that diffusion is always dominant in the DDC process. As illustrated in Section 2.3, this condition is required to successfully reproduce thermohaline stratification.

The results in Sections 3.1-3.5 also provide a new insight that has never been reported before but can better understand field observations. That is, though layer-merging could be very slow in real mine water bodies due to an unchanged layer number lasting for a long time (Reichart et al., 2011), the layer-merging process is always in progress. For thermohaline stratification observed in different flooded mines, the only difference for the development of thermohaline stratification in those mines is that the stratified temperature and salinity need different time-scales to evolve and then approach a quasi-equilibrium state with either a linear or a uniform distribution (one layer). In this state, the water temperature at the top, i.e., close to the ground surface, eventually increases to a higher value compared to the original one due to the water mixing caused by the dynamic layer-merging events. This is, in fact, advantageous to the efficiency of the geothermal energy

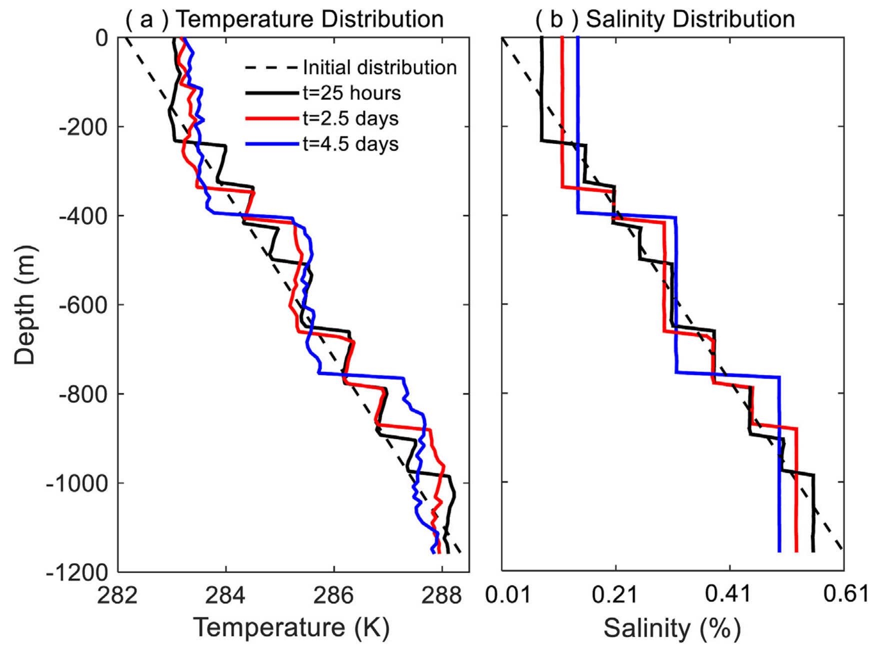

Fig. 12. Three cases with different layer numbers for the prediction of the initial distributions.

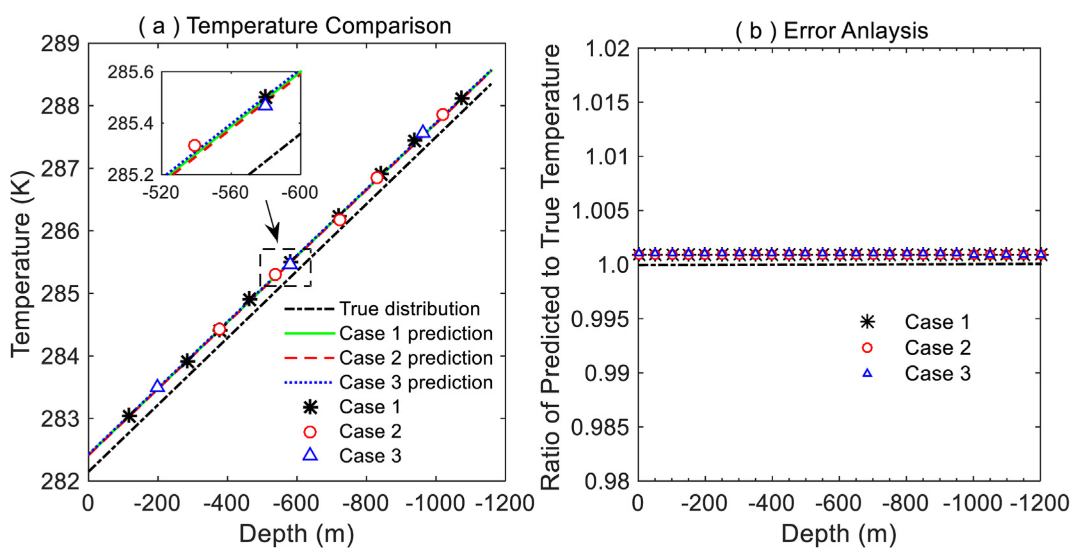

Fig. 13. Predictions of the initial temperature distribution: (a) temperature comparison and (b) error analysis.

application.

4.2. From theory to better evaluate and facilitate future real implementations

From a practical perspective, it is significant to accurately predict the future development of thermohaline stratification in real flooded mines for better engineered heat extraction. This is because the development of thermohaline stratification and the geothermal energy system can interact with each other in a complicated way to determine the overall performance of the geothermal energy system. Thermohaline stratification determines mine water temperatures available to heat pumps and consequently determines the efficiency of the geothermal energy system. It is also responsible for the water temperature distribution (i.e., the layered water structure), which affects the selection of water pumping locations.

In return, the selection of water pumping locations and pumping rates will influence the evolution of thermohaline stratification by altering the water temperature and its variations. Therefore, thermohaline stratification plays an important role in real energy applications; as a result, accurately predicting its development is particularly significant. As emphasized in Section 3.6, predicting the initial distributions of temperature and salinity is essentially needed for this purpose. Based on the initial conditions predicted with the proposed approach, the current layered water structure in real flooded mines can be reproduced to very closely real conditions. Based on that, future water temperature distributions (i.e., the layered water structure) could be accurately predicted. By

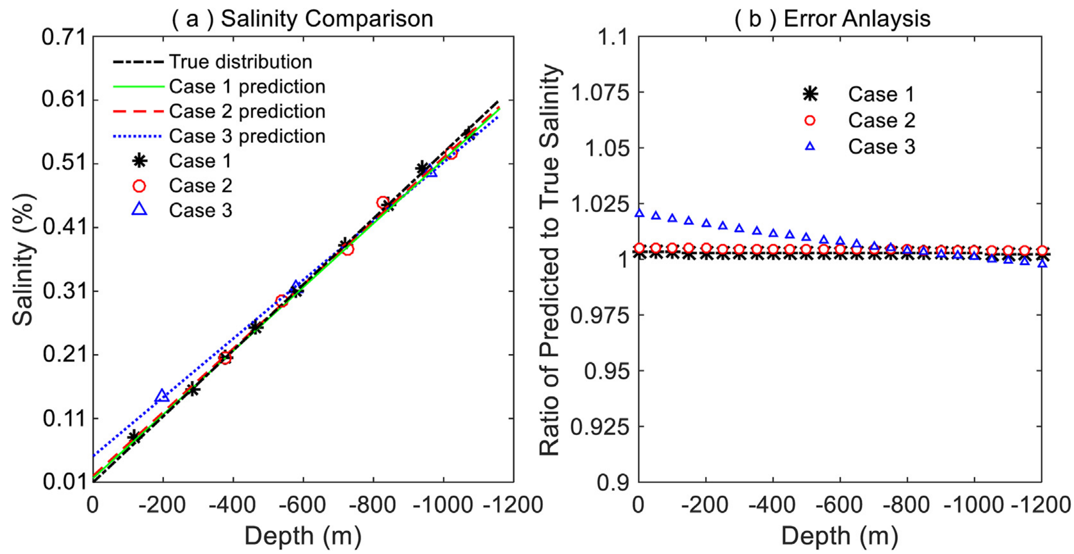

Fig. 14. Predictions of the initial salinity distribution: (a) salinity comparison and (b) error analysis.

contrast, thermohaline stratification predicted with other initial conditions based on random assumptions could not be that accurate; as a result, the predicted development of thermohaline stratification could not be used for precisely evaluating the interaction between the natural water system and the geothermal energy system.

4.3. Recommendations for better geothermal system designs

A good design of the geothermal energy system can be achieved based on the simulation results obtained in Sections 3.1-3.5 for more efficient heat extraction in the following ways.

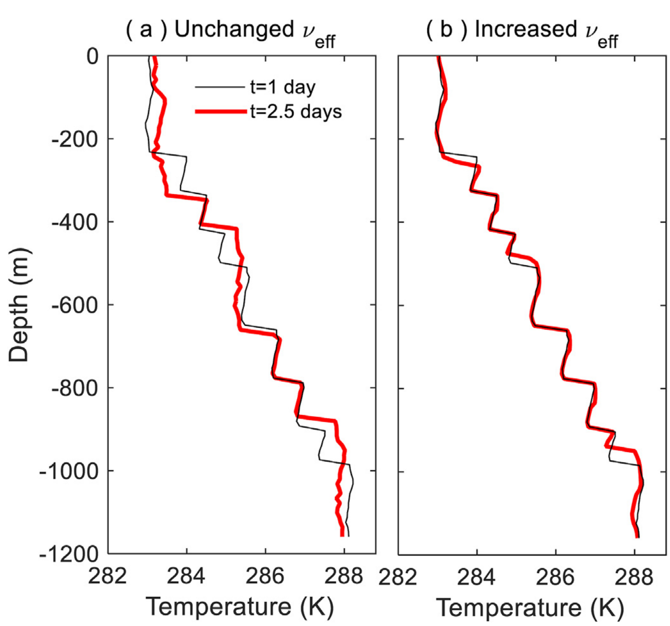

Fig. 15. Comparisons of temperature layers: (a) $\nu_{eff} = 3.95 \times 10^{-3}$ m^2/s and (b) ν_{eff} increases from 3.95×10^{-3} m^2/s to 1.25×10^{-2} m^2/s. The slim black line at $t = 1$ day was obtained when $\nu_{eff} = 3.95 \times 10^{-3}$ m^2/s, which serves as the initial condition for the situation in (b) when ν_{eff} increases to 1.25×10^{-2} m^2/s.

First, the efficiency of the geothermal energy system is determined by the water pumping location and the pumped water temperature. To enhance the system's efficiency, it is better to select a pumping location with high water temperatures. This can be achieved by selecting the pumping location in a lower water layer at a deeper depth, e.g., the third layer in Fig. 15a between 400 m and 600 m. However, the economic depth limit for pumping water from mines is about 305 m (Liu et al., 2015), beyond which the pumping cost could exceed the economic gain from the geothermal energy supply. Therefore, pumping water at a deeper depth to enhance the system's efficiency is only economic under the conditions that at least two layers exist within this depth limit; meanwhile, the temperature difference between an upper layer and any lower layers is significant, e.g., 3–5 K. Otherwise, it is better to keep the pumping location in the upper water layer to save pumping cost. In fact, the efficiency of the geothermal energy system is also directly influenced by layer-merging discussed here. As indicated by this study in Sections 3.1-3.5, layer-merging is a unique characteristic in thermohaline stratification. Meanwhile, this characteristic determines the variation of the temperature distribution. A quicker layer-merging process is beneficial to heat extraction. This is because pumping locations are usually in upper water layers close to the ground due to economic considerations. If layers merge quickly, the warm water in lower layers will move up quickly to heat the relatively cold water in upper layers, which can eventually increase future water temperatures available to heat pumps in upper water layers.

Second, it is possible to expedite layer-merging in practice by altering the transport parameters in multiple ways. Considering that the effective kinematic viscosity ν_{eff} affects thermohaline stratification more significantly than the other two parameters, reducing ν_{eff} may be a feasible way to speed up layer-merging (see Fig. 6). This could be achieved by adding chemical solutions in mine water during heat extraction. Another feasible way is to reduce the buoyancy ratio N. As indicated in Section 3.4, if values of N across the neighboring layers are small, the interfaces of these layers are relatively "weak" and eroded first. Heat extraction can naturally increase the temperature difference between the water layer where the pumping location is selected (i.e., the water pumping layer) and the neighboring layer. As indicated in Eq. (6), increasing the temperature difference will decrease N. Besides that, adding the eco-friendly solute (e.g., salts) to the pumped mine water after heat extraction can decrease the salinity difference between the water pumping layer and the neighboring layer. This can further reduce N across the water pumping layer and the neighboring layer, so that the layer interface can become "weaker" and disappear more quickly than that without adding the solute.

Finally, the pumping rate, which is a critical parameter in the geothermal energy system to determine the system's overall coefficient of performance (Al-Habaibeh et al., 2018), can also be regulated to improve the system's performance. For extracting heat via widely used open-loop heat pump systems (e.g., Al-Habaibeh et al. (2018) and Bao et al. (2019)), the pumping rate determines the rate of pumping water out (to an external heat exchanger) and sending it back into the mine-water-geologic-formation system (after heat extraction). At the pumping locations, the water velocity caused by the pumping action is usually higher than the water velocity in the natural water movement. This pumping-induced velocity can significantly accelerate the water mixing and consequently expedite the natural layer-merging process dominated by either the buoyancy ratio (see Figs. 9 and 10) or the effective kinematic viscosity ν_{eff} (see Figs. 6 and 15). In particular, the layer-merging process will become much quicker when a higher pumping rate (e.g., 0.03 m^3/s (Athresh et al., 2016)) is employed compared with a typically used pumping rate of 0.00082 m^3/s (Bao et al., 2019). This is because a high pumping rate can make the pumping-induced velocity exceed the water velocity in the natural water movement (about 10^{-2} m/s (Wolkersdorfer, 2008)) by one to two orders. This indicates that the selection of pumping rates can dominate over the two dominant factors ν_{eff} and N to control the speed of layer-merging in the region in the vicinity of pumping locations, even possibly the whole water region. Therefore, the selection of relatively high pumping rates is beneficial to enhancing the system's overall coefficient of performance by speeding up the layer-merging process.

However, it is worthwhile to note that the selection of high pumping rates, especially those with very high values (e.g., 0.063 m^3/s (Raymond and Therrien, 2014)), could change the layered water structure quickly, which might lead to a temperature reduction in mine water very rapidly. This adversely influences the sustainability of the whole geothermal energy system. Future work is thus needed to evaluate the variations of water temperatures with different pumping rates by modeling heat extraction. Also, environmental issues that might be triggered by the above techniques to make layer-merging quicker. This is because heavy metals are usually sealed at lower portions of water in mine shafts (Akcil and Koldas, 2006; Bao et al., 2018b; Hilson, 2000). Such contaminants can also be pumped to upper locations of shafts during heat extraction. Since either groundwater or surface water is connected to mine water and is water resources to flood mining spaces (Mativenga and Marnewick, 2018), expediting layer-merging may contaminate groundwater and surface water. Environmental issues thus must be carefully evaluated before real implementations.

5. Conclusions

This study addresses six unresolved issues for understanding the layered structure dominated by thermohaline stratification in large bodies of mine water. Based on the multiphysics simulations, the following conclusions can be drawn.

The key transport parameters, i.e., effective thermal diffusivity, effective kinematic viscosity, and diffusivity ratio, determine the layer formation speed and the layer-merging speed, in which the effect of the effective kinematic viscosity is more significant than that of other two parameters investigated here.

In layer merging, not all the layers merge simultaneously in common with the erosion of their interfaces. In fact, relatively "weak" interfaces are eroded and disappear first. These interfaces are relatively "weak" because the buoyancy ratios across them are smaller than those of not "weak" ones.

The buoyancy ratio determines the layer number in thermohaline stratification. The layer number increases with an increase in the buoyancy ratio. However, the smaller the buoyancy ratio, the greater the layer thickness.

An approach was proposed to predict initial linear temperature and salinity distributions, which are needed for predicting the present and future thermohaline stratification. The evaluation results confirmed the feasibility of the predictions of the initial distributions and proved the high reliability and accuracy of the proposed approach. The predictions of the thermohaline stratification evolution with the predicted initial conditions are more accurate than those with random assumptions to evaluate the interaction between the natural water system and the geothermal energy system.

This study provides in-depth insights to understand the layered water structure in flooded mines by addressing the above six issues, which have never been considered in existing geothermal energy applications with mine water. These insights can not only scientifically explain field observations, but also offer scientific bases for designing more efficient geothermal systems for mine water and any other types of subterranean water bodies.

The simulation results also led to recommendations for enhancing the system's efficiency. Techniques suggested by the simulations include changing transport parameters in mine water bodies, decreasing the buoyancy ratio by adding the eco-friendly solute to the pumped mine water, and selecting relatively high pumping rates. Such techniques can speed up layer-merging so that the relatively warm water in the lower layers can easily move up to increase the present and future water temperatures available to heat pumps in the upper water layers. The selection of water pumping locations in a lower water layer with a higher temperature is recommended if such pumping locations are within an economic limit depth. Beyond this limit depth, it is not economic for selecting pumping locations at a deeper water depth to enhance the system's efficiency. Further work is also needed for good engineering design of geothermal energy systems by understanding the interaction between geothermal energy systems and the natural water system via real heat extraction simulations.

CRediT authorship contribution statement

Ting Bao: Conceptualization, Methodology, Data curation, Writing - original draft. **Han Cao:** Formal analysis. **Yinghong Qin:** Writing - review & editing, Methodology. **Guosheng Jiang:** Writing - review & editing. **Zhen (Leo) Liu:** Supervision.

Declaration of competing interest

The authors declare there is no conflict of interest related to this work. The authors declare that they do not have any commercial interests that represent a conflict of interest in connection with the work.

Acknowledgments

This research is supported by the open research fund program of key laboratory of metallogenic prediction of nonferrous metals and geological environment monitoring (Central South University), Ministry of Education.

References

Akcil, A., Koldas, S., 2006. Acid Mine Drainage (AMD): causes, treatment and case studies. J. Clean. Prod. 14 (12-13), 1139–1145.
Al-Habaibeh, A., Athresh, A.P., Parker, K., 2018. Performance analysis of using mine water from an abandoned coal mine for heating of buildings using an open loop based single shaft GSHP system. Appl. Energy 211, 393–402.
Athresh, A.P., Al-Habaibeh, A., Parker, K., 2016. The design and evaluation of an open loop ground source heat pump operating in an ochre-rich coal mine water environment. Int. J. Coal Geol. 164, 69–76.
Bailey, M., Gandy, C., Watson, I., Wyatt, L., Jarvis, A., 2016. Heat recovery potential of mine water treatment systems in Great Britain. Int. J. Coal Geol. 164, 77–84.
Bakhtavar, E., Aghayarloo, R., Yousefi, S., Hewage, K., Sadiq, R., 2019. Renewable energy based mine reclamation strategy: a hybrid fuzzy-based network analysis. J. Clean. Prod. 14 (3), 349–365.
Bao, T., Liu, Z., 2016. Large-scale thermo-hydrodynamic modeling of a flooded underground mine for geothermal applications. In: Geo-Chicago 2016. ASCE, pp. 72–83.
Bao, T., Liu, Z., 2019a. Geothermal energy from flooded mines: modeling of transient energy recovery with thermohaline stratification. Energy Convers. Manag. 199, 111956.
Bao, T., Liu, Z., 2019b. Thermohaline stratification modeling with double-diffusive convection for geothermal energy recovery from flooded mines. Appl. Energy 237, 566–580.
Bao, T., Liu, Z., Meldrum, J., Green, C., 2018a. Large-scale mine water geothermal applications with abandoned mines. In: GeoShanghai International Conference. Springer, Shanghai, pp. 685–695.
Bao, T., Liu, Z., Meldrum, J., Green, C., Xue, P., Vitton, S., 2018b. Field tests and multiphysics analysis of a flooded shaft for geothermal applications with mine water. Energy Convers. Manag. 169, 174–185.
Bao, T., Meldrum, J., Vitton, C.G.S., Liu, Z., Bird, K., 2019. Geothermal energy recovery from deep flooded copper mines for heating. Energy Convers. Manag. 183, 604–616.
Behrooz, B.S., Elianne, D., Jan-Jaap, V.B., 2008. Geothermal use of deep flooded mines. In: International Symposium on Post-Mining. ISPM, Nancy, France, pp. 1–10.
Brandt, A., Fernando, H., 1995. Double-diffusive Convection. American Geophysical Union, Washington DC.
Burke, T., 2002. The use in Scotland of flooded mine workings as a source of geothermal energy. Geotherm. Energy Undergr. Min. 191–200.
Burnside, N., Banks, D., Boyce, A., 2016a. Sustainability of thermal energy production at the flooded mine workings of the former Caphouse Colliery, Yorkshire, United Kingdom. Int. J. Coal Geol. 164, 85–91.
Burnside, N., Banks, D., Boyce, A., Athresh, A., 2016b. Hydrochemistry and stable isotopes as tools for understanding the sustainability of minewater geothermal energy production from a ‘standing column’heat pump system: markham Colliery, Bolsover, Derbyshire, UK. Int. J. Coal Geol. 165, 223–230.
Butler, B.S., Burbank, W.S., 1929. The Copper Deposits of Michigan. US Government Printing Office.
Carpenter, J., Sommer, T., Wüest, A., 2012. Simulations of a double-diffusive interface in the diffusive convection regime. J. Fluid Mech. 711, 411–436.
Esen, M., Yuksel, T., 2013. Experimental evaluation of using various renewable energy sources for heating a greenhouse. Energy Build. 65, 340–351.
Farr, G., Sadasivam, S., Watson, I.A., Thomas, H.R., Tucker, D., 2016. Low enthalpy heat recovery potential from coal mine discharges in the South Wales Coalfield. Int. J. Coal Geol. 164, 92–103.
Hall, A., Scott, J.A., Shang, H., 2011. Geothermal energy recovery from underground mines. Renew. Sustain. Energy Rev. 15 (2), 916–924.
Han, H., Kuehn, T.H., 1991a. Double diffusive natural convection in a vertical rectangular enclosure I. Experimental study. Int. J. Heat Mass Tran. 34 (2), 449–459.
Han, H., Kuehn, T.H., 1991b. Double diffusive natural convection in a vertical rectangular enclosure II. Numerical study. Int. J. Heat Mass Tran. 34 (2), 461–471.
Hilson, G., 2000. Pollution prevention and cleaner production in the mining industry: an analysis of current issues. J. Clean. Prod. 8 (2), 119–126.
Hull, J.R., Nielsen, J., Golding, P., 1988. Salinity Gradient Solar Ponds. CRC Press Inc, Boca Raton, FL, USA.
Jardón, S., Ordóñez, A., Alvarez, R., Cienfuegos, P., Loredo, J., 2013. Mine water for energy and water supply in the central coal basin of asturias (Spain). Mine Water Environ. 32 (2), 139–151.
Jessop, A., 1995. Geothermal Energy from Old Mines at Springhill, pp. 463–468. Nova Scotia, Canada. Nova Scotia, Canada.
Johnson, K., Younger, P., 2002. Hydrogeological and geochemical consequences of the abandonment of Frazer's Grove carbonate hosted Pb/Zn fluorspar mine. North Pennines, UK Geol. Soc. 198 (1), 347–363. London, Special Publications.
Kories, H., Rüterkamp, P., Sippel, M., 2004. Field and numerical studies of water stratification in flooded shafts. In: Proceedings International Mine Water Association Symposium. IMWA, Newcastle upon Tyne, UK, pp. 149–159.
Ladwig, K.J., Erickson, P., Kleinmann, R., Posluszny, E., 1984. Stratification in Water Quality in Inundated Anthracite Mines, Eastern Pennsylvania. Pittsburgh Research Center, Pittsburgh, PA, USA.
Liu, Z., Meldrum, J., Xue, P., Green, C., 2015. Preliminary studies of the use of abandoned mine water for geothermal applications. In: IFCEE 2015. ASCE, pp. 1678–1690.
Loredo, C., Ordóñez, A., Garcia-Ordiales, E., Álvarez, R., Roqueñi, N., Cienfuegos, P., Peña, A., Burnside, N., 2017. Hydrochemical characterization of a mine water geothermal energy resource in NW Spain. Sci. Total Environ. 576, 59–69.
Love, A.J., Simmons, C.T., Nield, D.A., 2007. Double-diffusive convection in groundwater wells. Water Resour. Res. 43 (8), 1–11.
Luo, J., Luo, Z., Xie, J., Xia, D., Huang, W., Shao, H., Xiang, W., Rohn, J., 2018. Investigation of shallow geothermal potentials for different types of ground source heat pump systems (GSHP) of Wuhan city in China. Renew. Energy 118, 230–244.
Mativenga, P.T., Marnewick, A., 2018. Water quality in a mining and water-stressed region. J. Clean. Prod. 171, 446–456.
Menéndez, J., Ordóñez, A., Álvarez, R., Loredo, J., 2019. Energy from closed mines: underground energy storage and geothermal applications. Renew. Sustain. Energy Rev. 108, 498–512.
Menéndez, J., Ordónez, A., Fernández-Oro, J.M., Loredo, J., Díaz-Aguado, M.B., 2020. Feasibility analysis of using mine water from abandoned coal mines in Spain for heating and cooling of buildings. Renew. Energy 146, 1166–1176.
Oliveira, P.J., Issa, R.I., 2001. An improved PISO algorithm for the computation of buoyancy-driven flows. Numer. Heat Tran. Part B: Fundamentals. 40 (6), 473–493.
OpenFOAM, 2009. The Open Source CFD Toolbox. User Guide. OpenCFD Ltd, p. 770.
Radko, T., 2007. Mechanics of merging events for a series of layers in a stratified turbulent fluid. J. Fluid Mech. 577, 251–273.
Radko, T., Bulters, A., Flanagan, J., Campin, J.-M., 2014a. Double-diffusive recipes. Part I: large-scale dynamics of thermohaline staircases. J. Phys. Oceanogr. 44 (5), 1269–1284.
Radko, T., Flanagan, J., Stellmach, S., Timmermans, M.-L., 2014b. Double-diffusive recipes. Part II: layer-merging events. J. Phys. Oceanogr. 44 (5), 1285–1305.
Radosław, T., Uliasz-Misiak, B., 2019. Prospects for the use of carbon dioxide in enhanced geothermal systems in Poland. J. Clean. Prod. 229, 1189–1197.
Raymond, J., Therrien, R., 2014. Optimizing the design of a geothermal district heating and cooling system located at a flooded mine in Canada. Hydrogeol. J. 22 (1), 217–231.
Reichart, G., Vaute, L., Collon-Drouaillet, P., Buès, M.A., 2011. Modelling heat and salinity related convective processes in deep mining flooded wells. In: 11th International Mine Water Association Congress. IMWA, Aachen, Germany, pp. 183–187.
Rodríguez, R., Díaz, M.B., 2009. Analysis of the utilization of mine galleries as geothermal heat exchangers by means a semi-empirical prediction method. Renew. Energy 34 (7), 1716–1725.
Rottluff, F., 1998. Neue Warmepumpenanlage im Besucherbergwerk Zinngrube Ehrenfriedersdorf. Geotermische Energie 21, 811.
Sezai, I., Mohamad, A., 2000. Double diffusive convection in a cubic enclosure with opposing temperature and concentration gradients. Phys. Fluids 12 (9), 2210–2223.
Vallis, G.K., 2017. Atmospheric and Oceanic Fluid Dynamics. Cambridge University Press.
Watzlaf, G.R., Ackman, T.E., 2006. Underground mine water for heating and cooling using geothermal heat pump systems. Mine Water Environ. 25 (1), 1–14.
Wieber, G., Stemke, M., Wonik, T., Enzmann, F., Kersten, M., 2019. Stratification dynamics and geothermal potential of a deep shaft in the flooded Wolf Mine, Siegerland/Germany. Mine Water Environ. 38 (2), 325–334.
Wolkersdorfer, C., 2008. Water Management at Abandoned Flooded Underground Mines: Fundamentals, Tracer Tests, Modelling, Water Treatment. Springer Science & Business Media, München, Germany.
Zhang, C., Jiang, G., Jia, X., Li, S., Zhang, S., Hu, D., Hu, S., Wang, Y., 2019. Parametric study of the production performance of an enhanced geothermal system: a case study at the Qiabuqia geothermal area, northeast Tibetan plateau. Renew. Energy 132, 959–978.